Electrocatalysis

DOI: 10.1002/anie.201006644

Low-Platinum-Content Quaternary PtCuCoNi Nanotubes with Markedly Enhanced Oxygen Reduction Activity**

Lifeng Liu and Eckhard Pippel*

Polymer electrolyte membrane fuel cells (PEMFCs),[1] among other clean energy sources, represent a highly efficient and potentially inexpensive solution for worldwide ever-growing energy demand and increasing environmental concern, and are expected to be able to find various applications ranging from automotive vehicles to stationary and portable devices. Presently, the widespread commercialization of PEMFCs is, however, substantially hampered by the slow rate of the oxygen reduction reaction (ORR) at the cathode and the relatively high costs resulting from the excessive use of precious metal platinum. Therefore, considerable research efforts have recently been dedicated to the development of low-cost and highly efficient electrocatalysts for the ORR. While great progress has been made towards non-platinum electrocatalysts, such as nitrogen-doped carbon nanotubes/graphenes, conducting polymers, and other nonprecious metals/alloys,[2] platinum-based catalysts are still more efficient for the ORR. To date, there are several major strategies being developed to reduce the cost of platinum or enhance platinum utilization in electrocatalysts. The most popular one is to alloy Pt with other nonprecious metals, for example, Fe,[3] Co,[4] Ni,[5] Cu,[6] Ti,[7] Bi,[8] Sc, and Y[9] (PtM alloys). A variety of binary PtM alloy nanoparticle electrocatalysts have been investigated, and a 2–10-fold enhancement in ORR activity relative to pure Pt was repeatedly observed. It is generally accepted that this activity improvement can be ascribed to the lattice strain induced by the formation of Pt-skinned surfaces (i.e. PM alloy/Pt core/shell structure) through surface dealloying and the modified electronic structures, which can weaken the interaction between the Pt surface atoms and spectator species so as to increase the number of active Pt sites.[5a,6f] The second frequently used approach to enhancing Pt utilization is to design core/shell nanostructures by covering the surface of nonprecious metal nanocatalysts with a Pt shell or monolayer, which can be accomplished either by solution-phase heterogeneous nucleation and growth on nonprecious metal nanoparticles[10] or by Cu underpotential deposition and subsequent galvanic replacement reaction.[11] The third strategy is to use hollow Pt nanostructures as electrocatalysts.[12] In contrast to core–shell structures, the hollow geometry not only allows the reactants to access the external active Pt sites, but also renders the internal catalytically active sites accessible. Moreover, it was experimentally demonstrated very recently that the confinement effect occurring in the cavity of the nanocage catalysts can lead to a much higher frequency factor for the reduction of 4-nitrophenol by $NaBH_4$, a model reaction that can be used to evaluate the catalytic activity of metals.[13] So far, a few reports have been dedicated to the development of hollow Pt electrocatalysts for both the ORR and methanol oxidation reaction (MOR).[12] Nevertheless, in contrast with the other two approaches, Pt-based hollow electrocatalysts still remain insufficiently explored.

Herein, we report the synthesis of low-platinum-content quaternary PtCuCoNi nanotubes (NTs) by means of template-assisted, one-step electrodeposition and testing of the suitability of these hollow multimetallic NTs as effective ORR electrocatalysts. We found that the as-prepared PtCuCoNi NTs exhibit markedly enhanced ORR activity over commercially available Pt black and Pt/C catalysts because of compositional (i.e. multicomponent alloys) and geometrical (i.e. hollow structure) properties of the material.

The quaternary PtCuCoNi NTs were prepared by a one-step direct electrodeposition approach using a porous anodic aluminium oxide (AAO) membrane as the template. One-step electrodeposition takes advantage of the sputtered annular base electrode and rapid consumption of metal ions at the deposition front as a result of a large deposition current density to grow tubular structures (see Figure S1 in the Supporting Information) without the need to modify the pore walls of the AAO template, and has recently been proved to be a simple and highly efficient way to fabricate metallic and alloy nanotubes.[14] With this method, a growth rate of PtCuCoNi NTs of as high as 5 $\mu m\,min^{-1}$ was achieved. The electrodeposition was carried out under a condition that favors the reduction of less noble copper ions in the electrolyte (e.g. −0.8 V vs. Ag/AgCl). Afterwards, the AAO membrane was immersed into 10 wt% H_3PO_4 solution at 45 °C for 5 h. In this process, the porous alumina was completely removed. Meanwhile, mild dealloying also occurred in the as-deposited nanostructures.

Figure 1a shows a representative scanning electron microscopy (SEM) image of the as-prepared nanostructures after removal of the AAO template. Unlike the nanoporous PtCo and PtNi nanowires reported previously,[15] compact and robust fibers without discernable nanopores were observed after the acid treatment. Upon closer examination by transmission electron microscopy (TEM), it was found that most fibers actually possess hollow tubular morphology with an average diameter of 50 nm, as evidenced in Figure 1b,c. The

[*] Dr. L. Liu, Dr. E. Pippel
Max Planck Institute of Microstructure Physics
Weinberg 2, 06120 Halle (Saale) (Germany)
Fax: (+49) 345-551-1223
E-mail: liulif@mpi-halle.de

[**] We thank Dr. R. Scholz and Y. Huang for their assistance in the experiments.

Supporting information for this article is available on the WWW under http://dx.doi.org/10.1002/anie.201006644.

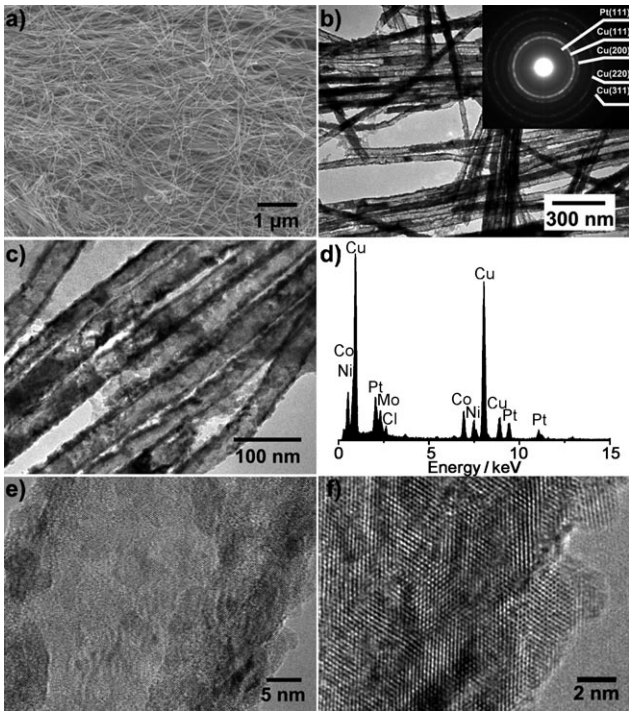

Figure 1. Structural characterization of the $Pt_5Cu_{76}Co_{11}Ni_8$ nanotubes. a) A representative SEM micrograph of the nanotubes released from AAO membranes. b,c) Typical TEM micrographs. Inset of (b): Electron diffraction pattern. d) EDX spectrum. e,f) High-resolution TEM images.

tube wall appears to be fairly rough, and its thickness ranges from 3 to 10 nm, which is a characteristic of NTs prepared by template-assisted one-step electrodeposition. It is noted that the tube diameter is virtually consistent with the pore diameter of the AAO template used. This might be associated with the fact that Cu is much more resistant under the present etching conditions, and its abundance in the NTs helps to preserve the tube diameter. It is also seen that some irregular holes exist along the NTs, probably resulting from either incomplete growth of the NTs due to the fast deposition[14] or the surface dealloying. It is worth mentioning that the roughened and porous surfaces of the NTs are particularly conducive to electrocatalysis because they not only offer a larger surface area but also allow the reactants to be transported into and within the NTs. Electron diffraction (ED) studies revealed that the NTs consist of multiple phases in which metallic Pt and Cu are distinguishable, as depicted in the inset of Figure 1b. This structural feature was also confirmed by X-ray diffraction (XRD) of the NT powders (Figure S2). Extensive energy-dispersive X-ray spectrum analyses revealed that the NTs are composed of Pt, Cu, Co, and Ni, and their atomic ratio turns out to be 5:76:11:8 (Figure 1d). Figure 1e,f shows typical high-resolution TEM images of the as-prepared $Pt_5Cu_{76}Co_{11}Ni_8$ NTs, indicating that the NTs are polycrystalline. Some distortions are visible in the lattice, which could originate from the surface dealloying.

We believe that the fast reduction of Cu^{2+} at the deposition front plays an essential role in the formation of the tubular structures. Control experiments showed that without the addition of Cu^{2+} to the electrolyte, only solid nanowires were obtained, even if other parameters (e.g. ion concentrations, deposition potential) were the same as those used for preparing $Pt_5Cu_{76}Co_{11}Ni_8$ NTs. Regarding the composition of the NTs, it is known that the standard reduction potentials for Cu^{2+}, Co^{2+}, and Ni^{2+} are $+0.34$ V, -0.28 V, and -0.25 V versus normal hydrogen electrode (NHE), respectively. The more positive reduction potential gives the Cu^{2+} ions a much higher tendency to be reduced, and therefore the content of Cu in the resulting NTs is much higher than that of Co and Ni, although their ion concentrations in the electrolyte are identical (0.25 M, see experimental section). In contrast, Co^{2+} and Ni^{2+} have similar reduction potentials and their concentrations in the electrolyte are the same; hence, their atomic percentages in the NTs are very close. In contrast, $[PtCl_6]^{2-}$ has a more positive reduction potential ($+0.68$ V vs. NHE) than Cu^{2+}, but the concentration of $[PtCl_6]^{2-}$ was 50 times lower than that of Cu^{2+} and its reduction to Pt requires two steps ($[PtCl_6]^{2-} \rightarrow [PtCl_4]^{2-} \rightarrow Pt$), so that only a small amount of Pt was incorporated into the NTs.

To get further insight into the elemental distribution in the as-prepared $Pt_5Cu_{76}Co_{11}Ni_8$ NTs, we carried out elemental analysis for a representative single NT by scanning transmission electron microscopy (STEM). Figure 2a shows a high-angle annular dark field (HAADF) micrograph of one NT, in which the porous tubular morphology can be clearly seen. Figure 2b–f depicts the elemental maps of Pt, Cu, Co, Ni, and their overlay. Although the tubular structure is no longer discernable as a result of the strong scattering and detector noise during scanning (as seen from the spots surrounding the NT), these maps disclose that all four elements are evenly distributed along the NT. It is also noted that the Pt map is not as dense as that of other elements, which could be ascribed to the very low content of Pt in the NT.

The electrocatalytic property of the supportless $Pt_5Cu_{76}Co_{11}Ni_8$ NTs was tested and compared with commercially available Pt black (BASF) and carbon-supported Pt nanoparticles (Pt/C, 30 wt% Pt on Vulcan XC-72, BASF) reference catalysts. Figure 3a shows the cyclic voltammograms (CVs) of these three catalysts dispersed on a glassy carbon electrode (GC, 5 mm in diameter, Pine Instruments), which were recorded in an Ar-saturated 0.1 M $HClO_4$ solution at room temperature. Before recording, the GC electrode was repeatedly swept from 0.05 V to 1.2 V until a steady CV curve was obtained (Figure S3).[16] From Figure 3a, it is seen that the CV profile of the $Pt_5Cu_{76}Co_{11}Ni_8$ NTs resembles that of Pt black and Pt/C, but the hydrogen adsorption/desorption peaks resulting from Pt (110) and Pt (100) crystal planes are not clearly visible, indicating that Pt may exist in one or few surface layers of the NTs in a disordered form. The electrochemically active surface area (ECSA) of the catalysts was calculated according to the hydrogen adsorption charges by using the conversion factor of 210 $\mu C\,cm^{-2}_{Pt}$. It was found that the ECSA is 14.7 $m^2\,g^{-1}_{Pt}$ for Pt black, 49.8 $m^2\,g^{-1}_{Pt}$ for Pt/C, and as high as 104.1 $m^2\,g^{-1}_{Pt}$ for the supportless $Pt_5Cu_{76}Co_{11}Ni_8$ NTs, respectively. The large ECSA of the $Pt_5Cu_{76}Co_{11}Ni_8$ NTs may stem from the following factors. First, it is assumed that

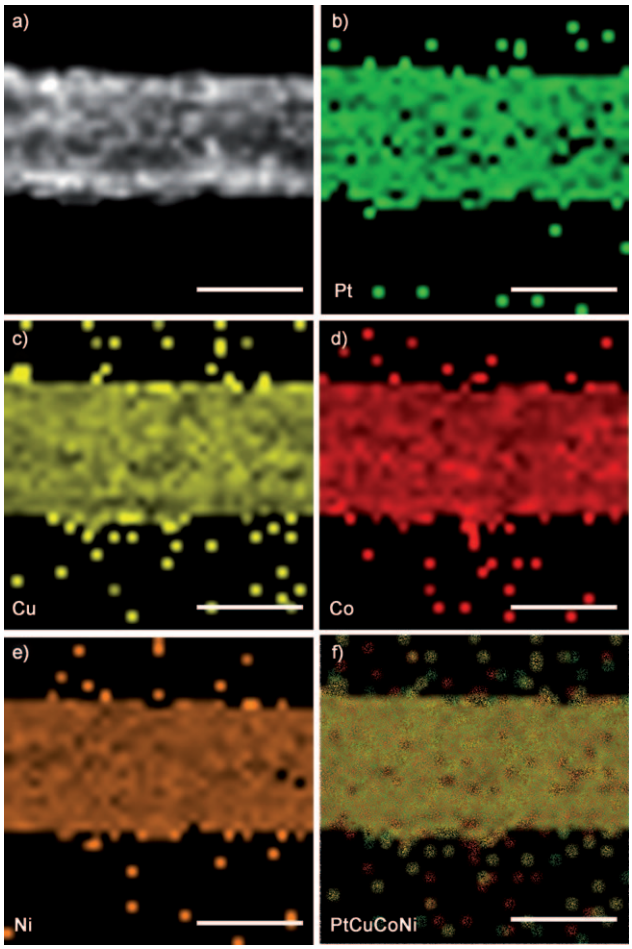

Figure 2. Elemental analyses of a typical single $Pt_5Cu_{76}Co_{11}Ni_8$ nanotube. a) HADDF image. Elemental maps of b) Pt, c) Cu, d) Co, and e) Ni. f) Overlay map of the elements. Scale bar: 30 nm.

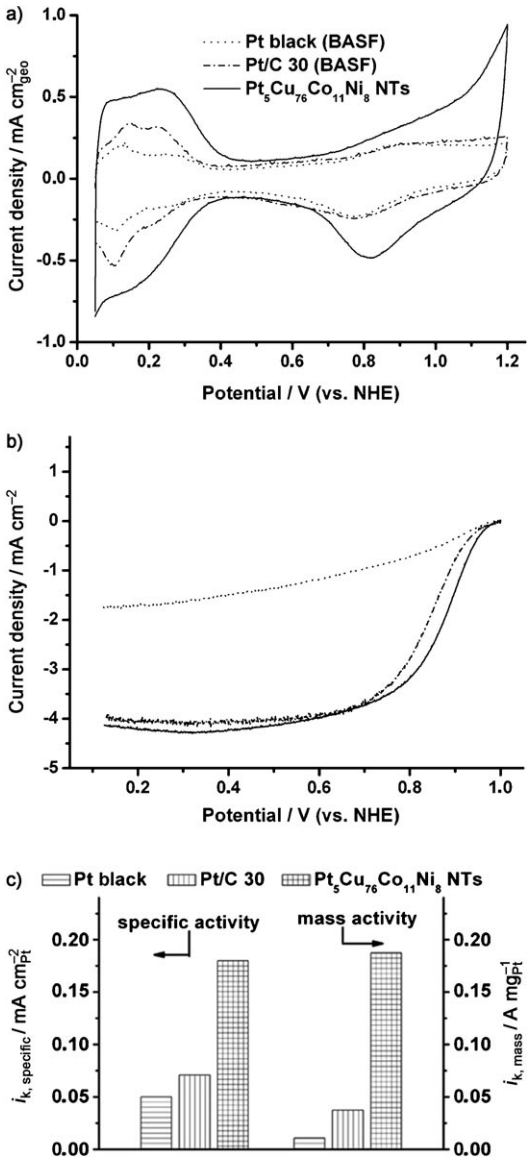

Figure 3. Evaluation of the electrocatalytic performance of the as-prepared $Pt_5Cu_{76}Co_{11}Ni_8$ nanotubes. Commercially available Pt black (BASF) and Pt/C catalysts (30 wt% Pt, BASF) were selected for comparison. The Pt loadings for Pt black, Pt/C, and $Pt_5Cu_{76}Co_{11}Ni_8$ nanotubes were 40.8 $\mu g\,cm^{-2}$, 11.2 $\mu g\,cm^{-2}$, and 11.2 $\mu g\,cm^{-2}$, respectively. a) Cyclic voltammograms recorded in Ar-saturated 0.1 M $HClO_4$ solution at a scan rate of 50 $mV\,s^{-1}$. b) Polarization curves recorded in O_2-saturated 0.1 M $HClO_4$ solution at a scan rate of 10 $mV\,s^{-1}$ and a revolution speed of 1600 rpm. c) Specific and mass activities of these three electrocatalysts at 0.9 V.

both the outer and inner surfaces of the NTs are covered with Pt atoms or at least are Pt-enriched as a result of surface dealloying,[6a–c] as evidenced by the Pt-like CV in Figure 3a, so that the limited content of Pt is fully utilized. Second, the unique tubular geometry with roughened outer and inner surfaces as well as porous tube walls not only enhances the active surface area but also makes all active sites accessible. We believe that it is the combination of these favorable factors that leads to the high ECSA of the $Pt_5Cu_{76}Co_{11}Ni_8$ NTs.

The hydrodynamic ORR activity of these three catalysts was evaluated by rotating disk electrode (RDE) voltammetry. Figure 3b compares the linear scan polarization curves of the Pt black, Pt/C, and $Pt_5Cu_{76}Co_{11}Ni_8$ NTs modified GC electrodes, which were recorded in O_2-saturated 0.1M $HClO_4$ at a revolution speed of 1600 rpm. According to Figure 3b, the half-wave potentials ($E_{1/2}$) for Pt black and Pt/C are 0.74 V and 0.84 V, respectively; in contrast, the $E_{1/2}$ value for $Pt_5Cu_{76}Co_{11}Ni_8$ NTs was found to be 0.87 V, indicating that the $Pt_5Cu_{76}Co_{11}Ni_8$ NTs have superior ORR performance over both Pt black and Pt/C catalysts. The kinetic current of the catalysts i_k was calculated from the Koutecky–Levich equation [Eq. (1)],[17] where i is the experimentally measured

$$i_k = \frac{i\,i_d}{i_d - i} \qquad (1)$$

current and i_d is the diffusion-limited current. Figure 3c compares the kinetic currents of these three catalysts at 0.9 V, normalized to the Pt surface area (specific activity) and Pt mass (mass activity). It reveals that the specific activity of $Pt_5Cu_{76}Co_{11}Ni_8$ NTs is about 0.18 $mA\,cm^{-2}{}_{Pt}$, which is 3.6 and 2.5 times higher than that of Pt black and Pt/C, respectively, indicating that the $Pt_5Cu_{76}Co_{11}Ni_8$ NTs are intrinsically

superior for ORR. Furthermore, the mass activity of $Pt_5Cu_{76}Co_{11}Ni_8$ NTs was also found to be as high as 0.19 A mg^{-1}_{Pt}, which is 17.5 and 5.0 times higher than that of Pt black and Pt/C catalysts, showing markedly enhanced ORR activity.

To further examine the reaction kinetics of oxygen reduction, the polarization curves of the supportless $Pt_5Cu_{76}Co_{11}Ni_8$ NTs modified GC electrode were recorded at different revolution speeds (ω, from 625 to 2025 rpm), as depicted in Figure S4. The corresponding Koutecky–Levich plots, namely j^{-1} as a function of $\omega^{-1/2}$, exhibit good linearity and are well parallel to each other, indicating that the ORR follows the first-order reaction kinetics relative to the dissolved oxygen. The calculated number of the transferred electrons during the reaction is 4.26, suggesting that the oxygen reduction of the $Pt_5Cu_{76}Co_{11}Ni_8$ NTs follows a four-electron pathway.

As for the origin of the markedly enhanced ORR activity of the $Pt_5Cu_{76}Co_{11}Ni_8$ NTs, it is believed that their large ECSA makes a major contribution to the improvement of mass activity, while the lattice strain induced by surface dealloying, which can result in the shortened Pt–Pt surface interatomic distances and modify the d band structure of the Pt atoms that can weaken the adsorption of spectacular reactive species,[6e] may play an indispensable role in the enhancement of specific activity. In addition, we assume that the unique combination of micrometer-sized length and hollow configuration of the NTs could also contribute to the enhanced ORR activity. Moreover, the highly conductive surface and network-like distribution of these NTs on the electrode surface can greatly improve the reaction kinetics relative to that of isolated Pt nanoparticles (for Pt black) or less conductive carbon support (for Pt/C), thus improving the activity. Also, as recently proposed by El-Sayed and co-workers,[13] the confinement effect of the reactions in hollow nanocatalysts with similar cavity sizes comes into play and can thereby result in a much enhanced catalytic performance.

In summary, quaternary PtCuCoNi nanotubes have been synthesized by a highly efficient template-assisted one-step electrodeposition approach. These nanotubes possess ultralow content of Pt, but nevertheless exhibit a markedly enhanced catalytic activity towards oxygen reduction relative to commercially available Pt black and Pt/C catalysts. The reaction kinetics study confirms that the oxygen reduction in PtCuCoNi nanotubes follows a four-electron pathway. The enhanced catalytic performance can be attributed to the combination of several favorable factors of these nanotubes: the multicomponent nature with which different elements could work synergistically, the strain and electronic effects associated with surface dealloying, and the unique hollow and porous geometry of the nanotubes. It is expected that these multimetallic PtCuCoNi nanotubes would be of great interest for use as low-platinum-content ORR catalysts in fuel cells. Furthermore, the combination of compositionally and geometrically favorable factors for ORR provides a new avenue in designing low-cost and highly efficient electrocatalysts.

Experimental Section

The AAO membranes were prepared by a two-step anodization process, as described in our previous work.[18] The average pore diameter of the as-obtained AAO membranes was 50 nm. The electrodeposition of PtCuCoNi quaternary nanotubes was accomplished in a three-electrode electrochemical cell at room temperature using the metal-coated AAO as working electrode and a platinum mesh and a Ag/AgCl electrode as counter and reference electrodes, respectively. The electrolyte consisted of 0.005 M $KPtCl_6$, 0.25 M $CuCl_2{\cdot}2H_2O$, 0.25 M $CoCl_2{\cdot}6H_2O$, 0.25 M $NiCl_2{\cdot}6H_2O$, and 0.485 M H_3BO_3. A potentiostat/galvanostat (PAR 263A) was employed to control the deposition. The deposition potential was set as −0.8 V vs. Ag/AgCl, at which Cu^{2+} ions are preferentially reduced. After electrodeposition, the AAO membrane was soaked into 10 wt% H_3PO_4 at 45 °C for 5 h. In this process, the alumina was completely dissolved; meanwhile, surface dealloying of the as-deposited PtCuCoNi nanotubes occurred, leading to roughened and porous surface of the nanotubes. The morphology and structure of the as-prepared $Pt_5Cu_{76}Co_{11}Ni_8$ nanotubes were characterized by scanning electron microscopy (SEM, JEOL 6701F) and transmission electron microscopy (TEM, JEOL 1010). The elemental analysis and high-resolution TEM investigation were carried out on a FEI Titan 80–300 microscope at an operating voltage of 300 keV. For electrochemical measurements, the catalyst inks were dispersed onto a glassy carbon electrode (GC, 5 mm diameter, Pine Instrumentation) and dried in air at room temperature. Subsequently, the GC electrode was covered with 10 μL 0.05% nafion (Sigma–Aldrich) solution and allowed to dry in air for 1 h. A rotating disk electrode (RDE, Pine Instrumentation) was used to study the hydrodynamic ORR activity of the catalysts. Both cyclic voltammograms and polarization curves were recorded with a PAR 263A potentiostat/galvanostat in 0.1 M $HClO_4$. A Pt wire and a double-junction Ag/AgCl electrode were utilized as counter and reference electrodes, respectively. All potentials, if not specified, are normalized to the normal hydrogen electrode (NHE) in this work.

Received: October 22, 2010
Revised: December 22, 2010
Published online: February 21, 2011

Keywords: alloys · electrochemistry · electrodeposition · nanotubes · template synthesis

[1] S. Litster, G. Mclean, *J. Power Sources* **2004**, *130*, 61.
[2] a) K. P. Gong, F. Du, Z. H. Xia, M. Durstock, L. M. Dai, *Science* **2009**, *323*, 760; b) M. Lefevre, E. Proietti, F. Jaouen, J. P. Godelet, *Science* **2009**, *324*, 71; c) R. Bashyam, P. Zelenay, *Nature* **2006**, *443*, 63; d) B. Winther-Jensen, O. Winther-Jensen, M. Forsyth, D. R. MacFarlane, *Science* **2008**, *321*, 671; e) Y. Shao, S. Zhang, M. H. Engelhard, G. Li, G. Shao, Y. Wang, J. Liu, I. A. Aksay, Y. Lin, *J. Mater. Chem.* **2010**, *20*, 7491; f) L. Qu, Y. Liu, J. B. Baek, L. Dai, *ACS Nano* **2010**, *4*, 1321; g) S. Tominaka, T. Hayashi, Y. Nakamura, T. Osaka, *J. Mater. Chem.* **2010**, *20*, 7175.
[3] a) A. K. Shukla, R. K. Raman, N. A. Choudhury, K. R. Priolkar, P. R. Sarode, S. Emura, R. Kumashiro, *J. Electroanal. Chem.* **2004**, *563*, 181; b) V. R. Stamenkovic, B. S. Mun, M. Arenz, K. J. J. Mayrhofer, C. A. Lucas, G. F. Wang, P. N. Ross, N. M. Markovic, *Nat. Mater.* **2007**, *6*, 241; c) J. Kim, Y. Lee, S. H. Sun, *J. Am. Chem. Soc.* **2010**, *132*, 4996.
[4] a) V. Stamenković, T. J. Schmidt, P. N. Ross, N. M. Markovic, *J. Phys. Chem. B* **2002**, *106*, 11970; b) P. Yu, M. Pemberton, P. Plasse, *J. Power Sources* **2005**, *144*, 11; c) S. Koh, J. Leisch, M. F. Toney, P. Strasser, *J. Phys. Chem. C* **2007**, *111*, 3744; d) Z. C. Liu, C. F. Yu, I. A. Rusakova, D. X. Huang, P. Strasser, *Top. Catal.* **2008**, *49*, 241; e) C. Wang, G. F. Wang, D. van der Vliet, K. C.

Chang, N. M. Markovic, V. R. Stamenkovic, *Phys. Chem. Chem. Phys.* **2010**, *12*, 6933.

[5] a) V. R. Stamenković, B. Fowler, B. S. Mun, G. F. Wang, P. N. Ross, C. A. Lucas, N. M. Markovic, *Science* **2007**, *315*, 493; b) V. R. Stamenković, T. J. Schmidt, P. N. Ross, N. M. Markovic, *J. Electroanal. Chem.* **2003**, *554*, 191; c) J. Zhang, H. Z. Yang, J. Y. Fang, S. Z. Zou, *Nano Lett.* **2010**, *10*, 638; d) J. B. Wu, J. L. Zhang, Z. M. Peng, S. C. Yang, F. T. Wagner, H. Yang, *J. Am. Chem. Soc.* **2010**, *132*, 4984.

[6] a) Z. Liu, S. Koh, C. Yu, P. Strasser, *J. Electrochem. Soc.* **2007**, *154*, B1192; b) P. Mani, R. Srivastava, P. Strasser, *J. Phys. Chem. C* **2008**, *112*, 2770; c) S. Koh, P. Strasser, *J. Am. Chem. Soc.* **2007**, *129*, 12624; d) S. Koh, N. Hahn, C. F. Yu, P. Strasser, *J. Electrochem. Soc.* **2008**, *155*, B1281; e) R. Z. Yang, J. Leisch, P. Strasser, M. F. Toney, *Chem. Mater.* **2010**, *22*, 4712; f) P. Strasser, S. Koh, T. Anniyev, J. Greeley, K. More, C. F. Yu, Z. C. Liu, S. Kaya, D. Nordlund, H. Ogasawara, M. F. Toney, A. Nilsson, *Nat. Chem.* **2010**, *2*, 454; g) D. Xu, Z. P. Liu, H. Z. Yang, Q. S. Liu, J. Zhang, J. Y. Fang, S. Z. Zou, K. Sun, *Angew. Chem.* **2009**, *121*, 4281; *Angew. Chem. Int. Ed.* **2009**, *48*, 4217; h) G. Gupta, D. A. Slanac, P. Kumar, J. D. Wiggins-Camacho, X. Q. Wang, S. Swinnea, K. L. More, S. Dai, K. J. Stevenson, K. P. Johnston, *Chem. Mater.* **2009**, *21*, 4515.

[7] Y. Kawasoe, S. Tanaka, T. Kuroki, H. Kusaba, K. Ito, Y. Teraoka, K. Sasaki, *J. Electrochem. Soc.* **2007**, *154*, B969.

[8] L. Demarconnay, C. Coutanceau, J. M. Leger, *Electrochim. Acta* **2008**, *53*, 3232.

[9] J. Greeley, I. E. L. Stephens, A. S. Bondarenko, T. P. Johansson, H. A. Hansen, T. F. Jaramillo, J. Rossmeisl, I. Chorkendorff, J. K. Norskov, *Nat. Chem.* **2009**, *1*, 552.

[10] a) Y. Wang, N. Toshima, *J. Phys. Chem. B* **1997**, *101*, 5301; b) S. Zhou, B. Varughese, B. Eichhorn, G. Jackson, K. McIlwrath, *Angew. Chem.* **2005**, *117*, 4615; *Angew. Chem. Int. Ed.* **2005**, *44*, 4539; c) S. Guo, J. Li, S. Dong, E. Wang, *J. Phys. Chem. C* **2010**, *114*, 15337.

[11] a) J. Zhang, F. H. B. Lima, M. H. Shao, K. Sasaki, J. X. Wang, J. Hanson, R. R. Adzic, *J. Phys. Chem. B* **2005**, *109*, 22701; b) M. Huang, Y. Jin, H. Jiang, X. Sun, H. Chen, B. Liu, E. Wang, S. Dong, *J. Phys. Chem. B* **2005**, *109*, 15264; c) M. H. Shao, K. Shoemaker, A. Peles, K. Kaneko, L. Protsailo, *J. Am. Chem. Soc.* **2010**, *132*, 9253.

[12] a) G. Chen, D. G. Xia, Z. R. Nie, Z. Y. Wang, L. Wang, L. Zhang, J. J. Zhang, *Chem. Mater.* **2007**, *19*, 1840; b) Z. W. Chen, M. Waje, W. Z. Li, Y. S. Yan, *Angew. Chem.* **2007**, *119*, 4138; *Angew. Chem. Int. Ed.* **2007**, *46*, 4060; c) H. M. Chen, R. S. Liu, M. Y. Lo, S. C. Chang, L. D. Tsai, Y. M. Peng, J. F. Lee, *J. Phys. Chem. C* **2008**, *112*, 7522; d) S. J. Guo, S. J. Dong, E. Wang, *Chem. Eur. J.* **2008**, *14*, 4689; e) Z. M. Peng, H. J. You, J. B. Wu, H. Yang, *Nano Lett.* **2010**, *10*, 1492.

[13] M. A. Mahmoud, F. Saira, M. A. El-Sayed, *Nano Lett.* **2010**, *10*, 3764.

[14] L. F. Liu, W. Y. Zhou, S. S. Xie, L. Song, S. D. Luo, D. F. Liu, J. Shen, Z. X. Zhang, Y. J. Xiang, W. J. Ma, Y. Ren, C. Y. Wang, G. Wang, *J. Phys. Chem. C* **2008**, *112*, 2256.

[15] a) L. F. Liu, E. Pippel, R. Scholz, U. Gösele, *Nano Lett.* **2009**, *9*, 4352; b) L. F. Liu, R. Scholz, E. Pippel, U. Gösele, *J. Mater. Chem.* **2010**, *20*, 5621.

[16] P. Strasser, S. Koh, J. Greeley, *Phys. Chem. Chem. Phys.* **2008**, *10*, 3670.

[17] B. Lim, M. Jiang, P. H. C. Camargo, E. C. Cho, J. Tao, X. M. Lu, Y. M. Zhu, Y. N. Xia, *Science* **2009**, *324*, 1302.

[18] L. Liu, W. Lee, Z. Huang, R. Scholz, U. Gösele, *Nanotechnology* **2008**, *19*, 335604.

